Local BVP methods for the computation of cell-face velocities in the incompressible Navier-Stokes equations

EINDHOVEN UNIVERSITY OF TECHNOLOGY
Department of Mathematics and Computer Science

CASA-Report 16-21
November 2016

Local BVP methods for the computation of cell-face velocities in the incompressible Navier-Stokes Equations

by

N. Kumar, J.H.M. ten Thije Boonkkamp, B. Koren

Centre for Analysis, Scientific computing and Applications
Department of Mathematics and Computer Science
Eindhoven University of Technology
P.O. Box 513
5600 MB Eindhoven, The Netherlands
ISSN: 0926-4507

Local BVP Methods for the Computation of Cell-Face Velocities in the Incompressible Navier-Stokes Equations

N. Kumar*, J.H.M. ten Thije Boonkkamp, B. Koren

Eindhoven University of Technology, P.O. Box 513, 5600 MB Eindhoven, The Netherlands

Abstract

The paper presents methods for the approximation of velocity components perpendicular to control-volume faces using local boundary value problems (BVPs). The computed cell-face velocity components depend on the local balance of convective and viscous forces, given by the grid Péclet number. The local BVP also includes the effects of the rotational behavior and the pressure gradient affecting the fluid flow across the interface of the control volume. The inclusion of these latter effects in the local BVP gives an accurate approximation of the velocity components. The method is free of numerical oscillations and introduces no or very little numerical dissipation into the system.

Keywords: finite-volume method, incompressible Navier-Stokes equations, convective terms, cell-face velocities

1. Introduction

In this paper we focus on the spatial discretization of the incompressible Navier-Stokes equations where the conservation laws are integrated over a disjoint set of control volumes. The semi-discrete system of equations requires velocity components to be approximated at the interface of the control volumes, particularly in the discrete convective terms. Commonly used methods for the approximation of these cell-face velocity components are the *central* and the *upwind* scheme. The central scheme approximates the velocity components by averaging the neighboring grid velocity components. The upwind scheme gives an approximation of the velocity components depending on the direction of the flow. Both methods have their trade-offs. The central scheme does not add any non-physical dissipation to the system, but may suffer from spurious oscillations, particularly at higher Reynolds numbers [1, 2]. On the other hand, the

*Corresponding author
Email address: n.kumar@tue.nl (N. Kumar)

upwind scheme yields good stability properties [3], but adds significant numerical dissipation to the system. An analysis of the energy-conservation properties of the two schemes can be found in [4]. Moreover, the above two methods for approximation of cell-face velocities are the limit case methods for the momentum equations, i.e., the central scheme results from the no-flow situation, whereas the upwind scheme corresponds to inviscid convection dominated flow.

An accurate approximation of the cell-face velocities should take into account the balance of the convective and viscous forces acting on the fluid. This issue can be tackled by the exponential/hybrid scheme described in [5, 6], which gives an approximation of the cell-face velocities as a weighted average of the central and the upwind scheme, with the weight function depending on the Péclet number (ratio of the convective and viscous forces).

Apart from the convective and viscous forces, the cell-face velocities are also affected by the pressure gradient and the effect of rotational behavior (quantitatively given by the gradient of the transverse flux or the cross-flux) of the fluid flow. In this paper we present methods for the computation of cell-face velocities using reduced momentum equations subject to suitable boundary conditions, reducing the problem to a local boundary value problem (BVP). This ensures that the computed cell-face velocities depend not only on the local balance of convective and viscous forces, but also on the pressure gradient and the gradient of the cross-flux. We aim to have an approximation method for cell-face velocities, which is accurate, free of numerical oscillations and introduces no or very little numerical dissipation to the system, without any significant increase in the computational cost.

The paper is organized as follows: In section 2 the finite-volume method is briefly described, giving a mathematical formulation for the computation of cell-face velocity components. In section 3, we derive an integral representation for the cell-face velocities by solving local BVPs. Sections 4 and 5 give the details about the closure of the model and iterative computation of the cell-face velocities. The numerical results for the local BVP methods are discussed in section 6 and conclusions are drawn in section 7.

2. Finite volume discretization

We consider the two-dimensional incompressible Navier-Stokes equations in primitive variable formulation, i.e.,

$$\nabla \cdot \boldsymbol{u} = 0, \tag{1a}$$

$$\frac{\partial \boldsymbol{u}}{\partial t} + \nabla \cdot (\boldsymbol{u}\boldsymbol{u}) = -\nabla p + \frac{1}{\mathrm{Re}} \nabla^2 \boldsymbol{u}, \tag{1b}$$

where $\boldsymbol{u} = u(x, y, t)\mathbf{e}_x + v(x, y, t)\mathbf{e}_y$, p and Re represent the velocity field, the pressure and the Reynolds number of the flow, respectively. The above system of equations is discretized using a second-order accurate finite-volume method

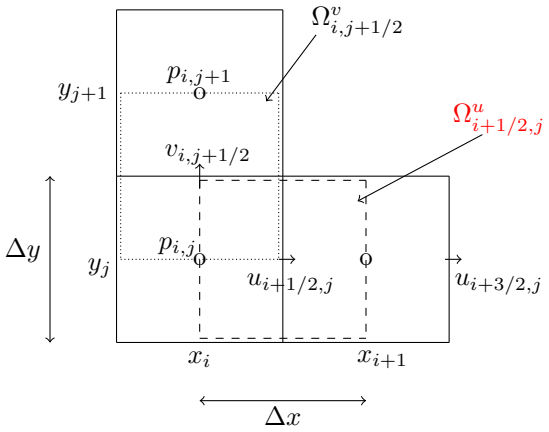

Figure 1: Control volumes for the spatial discretization of the momentum equations.

on a uniform staggered grid [7], as shown in figure 1. The semi-discrete incompressible Navier-Stokes equations can be written as

$$\mathbf{D}\mathbf{u} = \mathbf{r}_1(t), \tag{2a}$$

$$\boldsymbol{\Omega}\dot{\mathbf{u}}(t) = -\mathbf{N}(\mathbf{u}) + \frac{1}{\mathrm{Re}}\mathbf{L}\mathbf{u}(t) - \mathbf{G}\mathbf{p}(t) + \mathbf{r}_2(t), \tag{2b}$$

where $\dot{\mathbf{u}} = \partial\mathbf{u}/\partial t$ and $\mathbf{D}$, $\mathbf{N}$, $\mathbf{L}$ and $\mathbf{G}$ represent the discrete divergence, the non-linear convection, the viscous term and the gradient operator, respectively. The vector $\mathbf{r}_1$ gives the boundary conditions for the continuity equation (1a) and $\mathbf{r}_2$ contains the boundary conditions for the momentum equations (1b). The diagonal matrix $\boldsymbol{\Omega} = \mathrm{diag}(\Omega^u, \Omega^v)$ contains the volume/area of the u- and v-control volumes shown in figure 1. For the control volume $\Omega^u_{i+1/2,j}$, the u-component N^u of the discretized convection operator $\mathbf{N} = (N^u, N^v)$ is given by

$$\begin{aligned}\left(N^u(\mathbf{u})\right)_{i+1/2,j} =& \Delta y \left(u^2_{i+1,j} - u^2_{i,j}\right) + \\ & \Delta x \left((uv)_{i+1/2,j+1/2} - (uv)_{i+1/2,j-1/2}\right),\end{aligned} \tag{3}$$

where $(uv)_{i+1/2,j+1/2} = u_{i+1/2,j+1/2}v_{i+1/2,j+1/2}$ and $u_{i,j}$ is the numerical approximation of the velocity component $u(x_i, y_j)$. Similarly, for the v-control volume $\Omega^v_{i,j+1/2}$, the discrete convective operator $(N^v(\mathbf{u}))_{i,j+1/2}$ is given by

$$\begin{aligned}\left(N^v(\mathbf{u})\right)_{i,j+1/2} =& \Delta y \Big((uv)_{i+1/2,j+1/2} - (uv)_{i-1/2,j+1/2}\Big) + \\ & \Delta x \Big(v^2_{i,j+1} - v^2_{i,j}\Big).\end{aligned} \tag{4}$$

In order to compute $(N^u(\mathbf{u}))_{i+1/2,j}$ we need the velocity components $u_{i+1,j}$, $u_{i+1/2,j+1/2}$ and $v_{i+1/2,j+1/2}$, the rest can be computed in a similar manner.

These velocity components are not defined on the grid structure used for the discretization, and hence need to be approximated using neighboring grid velocities.

We begin with the approximation of the velocity component $u_{i+1,j}$, the approximation of the other cell-face velocity components is described in section 4. The central approximation of the velocity component $u_{i+1,j}$ is given by

$$u_{i+1,j} = \frac{1}{2}(u_{i+1/2,j} + u_{i+3/2,j}).$$

The upwind approximation depends on the direction of the flow and is defined as

$$u_{i+1,j} = \begin{cases} u_{i+1/2,j}, & \text{if } \; u_{i+1/2,j} > 0 \wedge u_{i+3/2,j} > 0, \\ u_{i+3/2,j}, & \text{if } \; u_{i+1/2,j} < 0 \wedge u_{i+3/2,j} < 0, \\ \frac{1}{2}(u_{i+1/2,j} + u_{i+3/2,j}), & \text{if } \; u_{i+1/2,j} u_{i+3/2,j} \leq 0. \end{cases}$$

We compute the velocity component $u_{i+1,j}$ by solving the momentum equation locally, such that the computed cell-face velocity component depends on the local Péclet number and source terms like the pressure gradient and the cross-flux gradient. Consider the steady u-momentum equation, i.e.,

$$(u^2)_x + (uv)_y = -p_x + \frac{1}{\mathrm{Re}}(u_{xx} + u_{yy}).$$

Restricting the solution of the above equation to the domain $x \in (x_{i+1/2}, x_{i+3/2})$, $y = y_j$, gives us the local BVP

$$(u^2 - \epsilon u_x)_x = -p_x - (uv - \epsilon u_y)_y, \;\; \epsilon = 1/\mathrm{Re}, \tag{5a}$$

$$u(x_{i+1/2}, y_j) = u_{i+1/2,j}, \quad u(x_{i+3/2}, y_j) = u_{i+3/2,j}. \tag{5b}$$

Figure 2 shows the domain and the boundary conditions involved in the computation of $u_{i+1,j}$, the details of which are given in the following section.

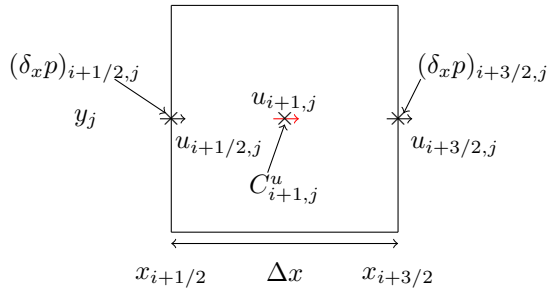

Figure 2: Control-volume for the computation of $u_{i+1,j}$

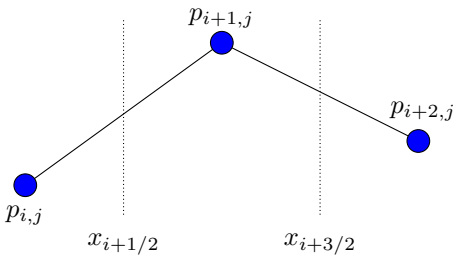

Figure 3: The piecewise linear pressure profile over the domain of the local BVP.

3. Integral representation of cell-face velocities

In this section we focus on the computation of $u_{i+1,j}$ from the local two-point BVP (5). Equation (5a) is a non-linear, inhomogeneous partial differential equation, which does not allow for exact representation of the solution. To simplify the problem, the non-linear term $(u^2)_x$ is linearized as Uu_x where U is an approximation of the velocity component $u_{i+1,j}$. Moreover, we assume that the gradient of the cross-flux $(uv-\epsilon v_y)_y$ is constant over the interval $(x_{i+1/2}, x_{i+3/2})$. We denote it by $C^u_{i+1,j}$. As a consequence of the staggered grid configuration, the discrete pressure profile is defined piecewise over $(x_{i+1/2}, x_{i+3/2})$, $y = y_j$. Further, we assume that the pressure p is *piecewise linear* over the domain of interest, making the pressure gradient p_x *piecewise constant*, as shown in figure 3. With the above assumptions, equation (5a) reduces to a linear, inhomogeneous, quasi-one-dimensional ordinary differential equation, given by

$$(Uu - \epsilon u_x)_x = -p_x - C^u_{i+1,j}, \;\; x_{i+1/2} < x < x_{i+3/2}, \; y = y_j. \tag{6}$$

In the following derivation we suppress the y-dependence of the local BVP, $u(x_i) := u(x_i, y_j)$, and introduce the following variables,

$$a := U/\epsilon, \qquad P := a\,\Delta x\,,$$

where $\Delta x = x_{i+3/2} - x_{i+1/2}$ and P is the grid Péclet number. Thus equation (6) can be rewritten as,

$$(u' - au)' = \frac{1}{\epsilon}(p' + C^u_{i+1,j}), \tag{7}$$

where $(.)' := (.)_x$. Since the pressure is assumed to be piecewise linear, we get that the pressure gradient p' is given by,

$$p'(x) = \begin{cases} (\delta_x p)_{i+1/2,j} = \frac{1}{\Delta x}(p_{i+1,j} - p_{i,j}), & x_{i+1/2} \le x \le x_{i+1}, \\ (\delta_x p)_{i+3/2,j} = \frac{1}{\Delta x}(p_{i+2,j} - p_{i+1,j}), & x_{i+1} < x \le x_{i+3/2}. \end{cases}$$

Integrating equation (7) we get

$$u' - au = \frac{1}{\epsilon}\Big(I_1(x) + C^u_{i+1,j}(x - x_{i+1}) + k_1\Big), \quad I_1(x) = \int_{x_{i+1}}^{x} p'(\xi)\mathrm{d}\xi\,, \tag{8}$$

where k_1 is the integration constant. Note that we integrated equation (7) from x_{i+1} to $x \in (x_{i+1/2}, x_{i+3/2})$, as the pressure gradient p' has a jump at $x = x_{i+1}$. Integrating equation (8) using the integrating factor formulation, $u' - au = e^{ax}(e^{-ax}u)'$ and invoking the left boundary condition $u(x_{i+1/2}) = u_{i+1/2}$, we get

$$\begin{aligned} u(x) =& e^{a(x-x_{i+1/2})}u_{i+1/2,j} + \frac{1}{\epsilon}\int_{x_{i+1/2}}^{x} e^{a(x-\zeta)} I_1(\zeta)\,\mathrm{d}\zeta + \\ & \frac{1}{\epsilon}C^u_{i+1,j}\int_{x_{i+1/2}}^{x} e^{a(x-\zeta)}(\zeta - x_{i+1})\,\mathrm{d}\zeta + \frac{1}{\epsilon}k_1\int_{x_{i+1/2}}^{x} e^{a(x-\zeta)}\,\mathrm{d}\zeta. \end{aligned} \tag{9}$$

We define the normalized coordinate σ on the interval $[x_{i+1/2}, x_{i+3/2}]$, given by

$$\sigma := \sigma(x) = \frac{x - x_{i+1/2}}{\Delta x}.$$

Using equation (9) and the normalized coordinate σ we get

$$\begin{aligned} u(\sigma) = e^{P\sigma}u_{i+1/2,j} + \frac{1}{\epsilon}\Delta x\, I_2(\sigma;P) + \frac{1}{\epsilon}C^u_{i+1,j}\,\Delta x^2\, I_3(\sigma;P) + \\ \frac{k_1}{\epsilon}\Delta x\,\sigma\varphi(P\sigma), \qquad \varphi(z) := \frac{e^z - 1}{z}, \end{aligned}$$

where the integral functions I_2 and I_3 are defined as

$$\begin{aligned} I_2(\sigma;P) &:= \int_0^\sigma e^{P(\sigma-\eta)} I_1(x_{i+1/2} + \eta\Delta x)\,\mathrm{d}\eta, \\ I_3(\sigma;P) &:= \int_0^\sigma e^{P(\sigma-\eta)}\big(\eta - \tfrac{1}{2}\big)\,\mathrm{d}\eta \\ &= \frac{1}{P^2}\big(\big(1 - \tfrac{1}{2}P\big)\big(e^{P\sigma} - 1\big) - \sigma P\big). \end{aligned}$$

Invoking the right boundary condition $u(x_{i+3/2}) = u_{i+3/2,j}$ we get

$$\begin{aligned} u(\sigma) =& \Gamma_1(1-\sigma;-P)u_{i+1/2,j} + \Gamma_1(\sigma;P)u_{i+3/2,j} + \frac{1}{\epsilon}\Delta x\big(I_2(\sigma;P) - \\ & \Gamma_1(\sigma;P)I_2(1;P)\big) + \frac{1}{\epsilon}C^u_{i+1,j}\Delta x^2\big(I_3(\sigma;P) - \Gamma_1(\sigma;P)I_3(1;P)\big), \end{aligned} \tag{10}$$

where

$$\Gamma_1(\sigma;P) := \frac{e^{P\sigma} - 1}{e^P - 1}.$$

The integral representation $u(\sigma)$ can be expressed as a sum of three parts, i.e.,

$$u(\sigma) = u^{\mathrm{h}}(\sigma) + u^{\mathrm{p}}(\sigma) + u^{\mathrm{c}}(\sigma), \tag{11a}$$

$$u^{\mathrm{h}}(\sigma) := \Gamma_1(1-\sigma;-P)u_{i+1/2,j} + \Gamma_1(\sigma;P)u_{i+3/2,j}, \tag{11b}$$

$$u^{\mathrm{p}}(\sigma) := \frac{1}{\epsilon}\Delta x\,\Big(I_2(\sigma;P) - \Gamma_1(\sigma;P)\,I_2(1;P)\Big), \tag{11c}$$

$$u^{\mathrm{c}}(\sigma) := \frac{1}{\epsilon}C^u_{i+1,j}\Delta x^2\,\Big(I_3(\sigma;P) - \Gamma_1(\sigma;P)\,I_3(1;P)\Big). \tag{11d}$$

Let

$$W(P) := (e^P + 1)^{-1},$$

be a weight function, satisfying $0 \leq W(P) \leq 1$ and $W(P) + W(-P) = 1$. In order to compute $u_{i+1,j}$, we set $\sigma = \frac{1}{2}$. Thus, $u^{\mathrm{h}}(\frac{1}{2})$ can be expressed as the weighted average of $u_{i+1/2,j}$ and $u_{i+3/2,j}$:

$$u^{\mathrm{h}}(\tfrac{1}{2}) = W(-P/2)u_{i+1/2,j} + W(P/2)u_{i+3/2,j}. \tag{12}$$

Computing the integral $I_2(\sigma; P)$ for $\sigma = 1/2$ and $\sigma = 1$, we get

$$\begin{aligned} I_2\big(\tfrac{1}{2}; P\big) &= \Delta x \left(p_{i+1,j} - p_{i,j}\right) \frac{1}{P^2}\big(\big(1 - \tfrac{1}{2}P\big)e^{P/2} - 1\big), \\ I_2(1; P) &= e^{P/2} I_2\big(\tfrac{1}{2}; P\big) + \Delta x \left(p_{i+2,j} - p_{i+1,j}\right)\big(e^{P/2} - 1 - \tfrac{1}{2}P\big). \end{aligned}$$

Defining

$$\Gamma_2(P) := \frac{e^P - 1 - P}{P^2(e^P + 1)},$$

and using the expressions for $I_2\big(\frac{1}{2}; P\big)$ and $I_2(1; P)$, $u^{\mathrm{p}}(\frac{1}{2})$ can be expressed as

$$u^{\mathrm{p}}\big(\tfrac{1}{2}\big) = -\frac{1}{4\epsilon}\Delta x^2\big(\Gamma_2(-P/2)(\delta_x p)_{i+1/2,j} + \Gamma_2(P/2)(\delta_x p)_{i+3/2,j}\big). \tag{13}$$

Lastly, $u^{\mathrm{c}}\big(\frac{1}{2}\big)$ is expressed as

$$u^{\mathrm{c}}\big(\tfrac{1}{2}\big) = -\frac{1}{4\epsilon}\Delta x^2 C^u_{i+1,j}\Gamma_3(P/2), \tag{14}$$

where

$$\Gamma_3(P) := \frac{e^P - 1}{P(e^P + 1)}.$$

From the expressions (12), (13) and (14), we get that the velocity component $u_{i+1,j}$ is given

$$u_{i+1,j} = u^{\mathrm{h}}(\tfrac{1}{2}) + u^{\mathrm{p}}(\tfrac{1}{2}) + u^{\mathrm{c}}(\tfrac{1}{2}). \tag{15}$$

Depending on the terms in the right-hand side of equation (7) we get three possible methods for computing $u_{i+1,j}$, viz., the *homogeneous* 1-*D local BVP method*, the *inhomogeneous* 1-*D local BVP method* and the 2-*D local BVP method*, specified below.

3.1. Homogeneous 1-*D local BVP method*

If we ignore the pressure gradient and the gradient of the cross-flux, then solving the homogeneous equation

$$(u' - au)' = 0, \tag{16}$$

gives the cell-face velocity component $u_{i+1,j}$ as a weighted average of $u_{i+1/2,j}$ and $u_{i+3/2,j}$ as in equation (12). This is the *homogeneous* 1-*D local BVP method*. Figure 4 shows the dependence of the function W on the Péclet number P.

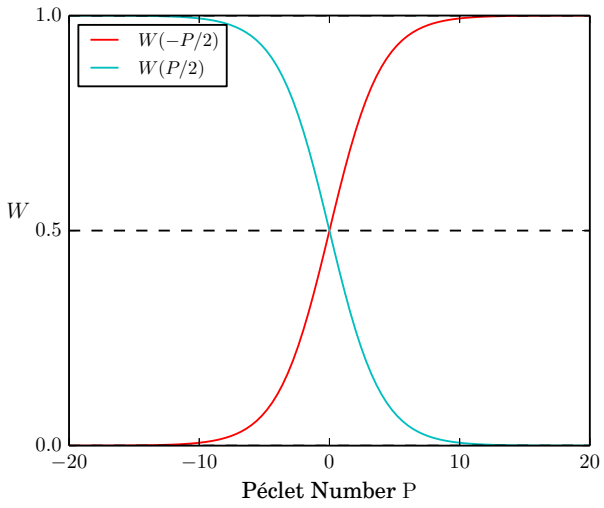

Figure 4: Functions $W = W(P/2)$ and $W = W(-P/2)$.

Note that for $P = 0$, $W(P/2) = W(-P/2) = 1/2$, thus we get that $u_{i+1,j}$ is the arithmetic average of $u_{i+1/2,j}$ and $u_{i+3/2,j}$ as in the central scheme. For $P > 10$ (or $P < -10$) we have $W(-P/2) \approx 1$ (or $W(P/2) \approx 1$), resulting in the upwind scheme. The homogeneous part can be expressed as a weighted average of the upwind and the central scheme:

$$u^{\mathrm{h}}(\tfrac{1}{2}) = (1 - 2W(|P|/2))u^{\mathrm{upwind}} + 2W(|P|/2)u^{\mathrm{central}}. \tag{17}$$

3.2. Inhomogeneous 1-D local BVP method

The inclusion of the pressure gradient results in the inhomogeneous differential equation,

$$(u' - au)' = -p', \tag{18}$$

in which case the cell-face velocity component is expressed as $u_{i+1,j} = u^{\mathrm{h}}(\frac{1}{2}) + u^{\mathrm{p}}(\frac{1}{2})$. The contribution of the discrete pressure gradients $(\delta_x p)_{i+1/2,j}$ and $(\delta_x p)_{i+3/2,j}$ to the component u^{p} is controlled by the function Γ_2. Figure 5 gives the dependence of $\Gamma_2(P/2)$ on the Péclet number. It can be seen that for $P = 0$, $(\delta_x p)_{i+1/2,j}$ and $(\delta_x p)_{i+3/2,j}$ have equal contribution. However as the Péclet number ($P > 0$) increases, we get that $\Gamma_2(-P/2) \to 2/P$ and $\Gamma_2(P/2) \to 4/P^2$, as $P \to \infty$, making the upwind pressure gradient $(\delta_x p)_{i+1/2,j}$ more dominant.

3.3. 2-D local BVP method

Finally, including both the pressure gradient and cross-flux gradient and solving differential equation (7), results in the cell-face velocity component given by equation (15). The term $u^{\mathrm{c}}(\frac{1}{2})$ is proportional to the cross-flux gradient $C^u_{i+1,j}$

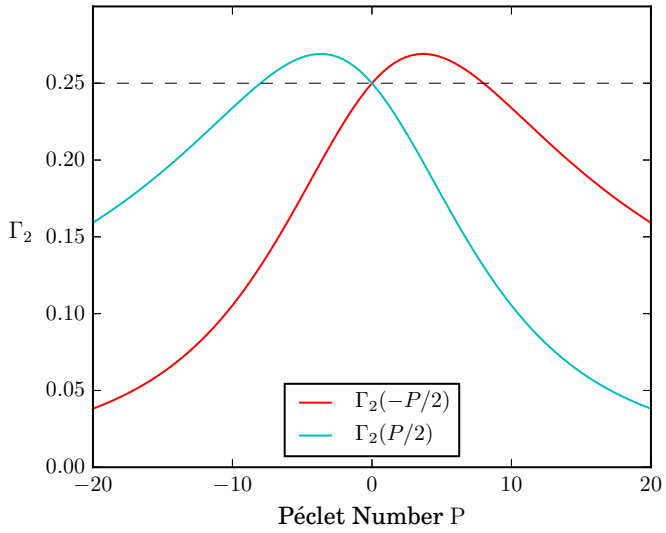

Figure 5: Function $\Gamma_2 = \Gamma_2(P/2)$.

and contains the factor $\Gamma_3(P/2)$ depending on the Péclet number. Figure 6 shows the variation in the values of $\Gamma_3(P/2)$ with the change of Péclet number. It can be observed that $\Gamma_3(P/2)$ attains its maximum for $P = 0$ and then asymptotically goes to 0 as $|P| \to \infty$.

Approximation of the gradient of the cross-flux
In order to compute the term $u^c(1/2)$ given by equation (14), we need the cross-flux gradient $C^u_{i+1,j}$. $C^u_{i+1,j}$ is computed using $C^u_{i+1/2,j}$ and $C^u_{i+3/2,j}$, which are approximations of the gradient $(uv - \epsilon u_y)_y$ at $(x_{i+1/2}, y_j)$ and $(x_{i+3/2}, y_j)$, respectively, with $C^u_{i+1/2,j}$ defined as

$$C^u_{i+1/2,j} = \frac{1}{\Delta y}\big((uv)_{i+1/2,j+1/2} - (uv)_{i+1/2,j-1/2}\big) - \frac{\epsilon}{\Delta y^2}\big(u_{i+1/2,j+1} - 2u_{i+1/2,j} + u_{i+1/2,j-1}\big).$$

The gradient $C^u_{i+3/2,j}$ can be computed similarly. Analogous to the homogeneous 1-D local BVP method, we compute $C^u_{i+1,j}$ as the weighted average:

$$C^u_{i+1,j} = W(-P/2)C^u_{i+1/2,j} + W(P/2)C^u_{i+3/2,j}.$$

4. Closure of the model

In the previous section, we presented integral representations for approximating the cell-face velocity component $u_{i+1,j}$. To compute the discrete convective operator $(N^u(\mathbf{u}))_{i+1/2,j}$ we also need $u_{i+1/2,j+1/2}$ and $v_{i+1/2,j+1/2}$. These velocity

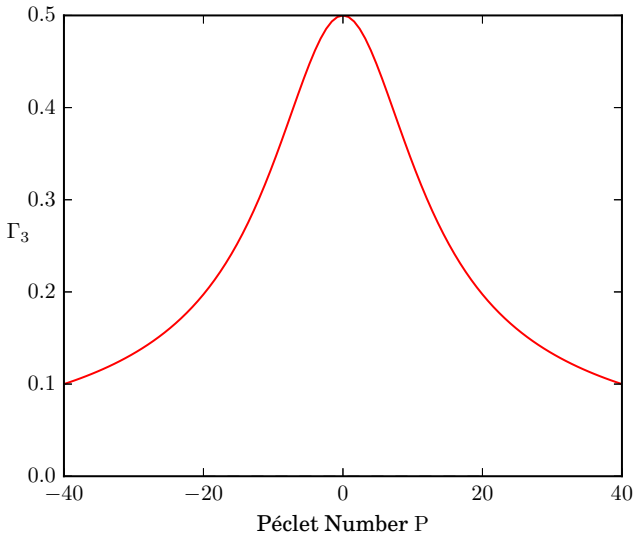

Figure 6: Function $\Gamma_3 = \Gamma_3(P/2)$.

components are also computed using local BVPs, as shown in figure 7. For computing both $u_{i+1/2,j+1/2}$ and $v_{i+1/2,j+1/2}$, we make use of the *homogeneous* 1-*D local BVP method* discussed in section 3. The velocity component $u_{i+1/2,j+1/2}$ is computed from the local boundary value problem :

$$Vu_y - \epsilon u_{yy} = 0, \qquad y_j \le y \le y_{j+1},\ x = x_{i+1/2}, \tag{19a}$$
$$u(x_{i+1/2}, y_j) = u_{i+1/2,j},\ \ u(x_{i+1/2}, y_{j+1}) = u_{i+1/2,j+1}, \tag{19b}$$

where V is an estimate for $v_{i+1/2,j+1/2}$. Likewise for $v_{i+1/2,j+1/2}$, we use the following local BVP :

$$Uv_x - \epsilon v_{xx} = 0, \qquad x_i \le x \le x_{i+1},\ y = y_{j+1/2}, \tag{20a}$$
$$v(x_i, y_{j+1/2}) = v_{i,j+1/2},\ \ v(x_{i+1}, y_{j+1/2}) = v_{i+1,j+1/2}, \tag{20b}$$

with U being an estimate for $u_{i+1/2,j+1/2}$. Note that equation (19a) is the linearized form of the equation

$$(uv)_y - \epsilon u_{yy} = 0,$$

which is the cross-flux gradient in the x-momentum equation. Similarly, equation (20a) is the linearized form of,

$$(uv)_x - \epsilon v_{xx} = 0,$$

which is the cross-flux gradient in the y-momentum equation.

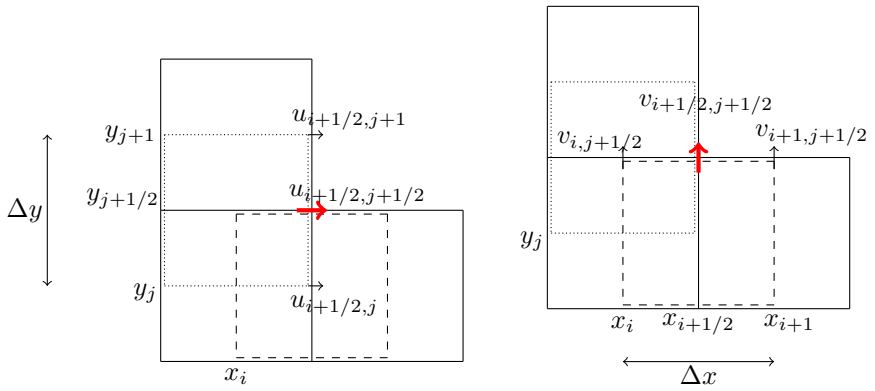

(a) Velocity component $u_{i+1/2,j+1/2}$. (b) Velocity component $v_{i+1/2,j+1/2}$.

Figure 7: Computation of other cell-face velocity components.

All the methods described so far are analogously applied for discretization of the convective term $\big(N^v(\mathbf{u})\big)_{i,j+1/2}$ given by equation (4). To compute the discretized operator $\big(N^v(\mathbf{u})\big)_{i,j+1/2}$, we need the velocity components $v_{i,j+1}$, $u_{i+1/2,j+1/2}$ and $v_{i+1/2,j+1/2}$. The velocity component $v_{i,j+1}$ is computed using the local BVP

$$(v' - bv)' = \frac{1}{\epsilon}(p' + C^v_{i,j+1}), \quad x = x_i,\ y_{j+1/2} \le y \le y_{j+3/2},$$
$$v(x_i, y_{j+1/2}) = v_{i,j+1/2}, \quad v(x_i, y_{j+3/2}) = v_{i,j+3/2},$$

where $(.)' := (.)_y$ and $b := V/\epsilon$, with V being an estimate for $v_{i,j+1}$. Solving the local BVP, as discussed in section 3, we can formulate $v_{i,j+1}$ as a sum of $v^{\mathrm{h}}(\frac{1}{2})$, $v^{\mathrm{p}}(\frac{1}{2})$ and $v^{\mathrm{c}}(\frac{1}{2})$. Similarly as $C^u_{i+1,j}$, the discrete cross-flux gradient $C^v_{i,j+1}$ is computed as the weighted average

$$C^v_{i,j+1} = W(-P^v/2)C^v_{i,j+1/2} + W(P^v/2)C^v_{i,j+3/2},$$

where the Péclet number P^v is defined as $P^v := V\Delta y/\epsilon$.

5. Iterative computation of the cell-face velocities

The discussion so far gave details about the derivation of an integral representation of the cell-face velocity components by solving a linearized local BVP. However, the local BVPs that we intend to solve are non-linear. To account for this non-linearity, the cell-face velocities are computed iteratively. Algorithm 1 gives the details of the iteration procedure.

For the iterative computation of $u_{i+1,j}$, we begin by making an estimate for U in the linearization of equation (5). Corresponding to this estimate we obtain the Péclet number given by $P = U\Delta x/\epsilon$, which is used to compute the velocity

component using one of the three methods described in the previous section. The computed cell-face velocity component is used to update the estimate U and the Péclet number and the procedure is repeated until the computed values converge to a given tolerance. The velocity components $u_{i+1/2,j+1/2}, v_{i+1/2,j+1/2}$ and $v_{i,j+1}$ are computed iteratively in a similar manner.

Initialization: Set $u^{\mathrm{h}} = \frac{1}{2}(u_{i+1/2,j} + u_{i+3/2,j})$, $u^{\mathrm{p}} = 0$ and $u^{\mathrm{c}} = 0$
$u_{i+1,j} = u^{\mathrm{h}} + u^{\mathrm{p}} + u^{\mathrm{c}}$

Set TOL as allowed maximum tolerance for convergence
Set error $>$ TOL

while error $\geq$ TOL **do**
  $u^{\mathrm{old}}_{i+1,j} = u_{i+1,j}$
  $P := \frac{1}{\epsilon} u_{i+1,j} \Delta x$
  Compute u^{h}, u^{p} and u^{c} from (12), (13) and (14), respectively
  $u_{i+1,j} = u^{\mathrm{h}} + u^{\mathrm{p}} + u^{\mathrm{c}}$
  error $= \left| u_{i+1,j} - u^{\mathrm{old}}_{i+1,j} \right|$
end while

Algorithm 1: Iteration to compute the cell-face velocity component $u_{i+1,j}$.

6. Numerical results

We now compare the local BVP methods with the central and upwind schemes for the following test cases: the Taylor-Green vortex problem and the standard lid-driven square cavity flow.

6.1. Taylor-Green vortex

The Taylor-Green vortex in two dimensions admits an exact solution to the incompressible Navier-Stokes equations, given by

$$u(x, y, t) = -\sin(\pi x)\cos(\pi y) e^{-2\pi^2 t/\mathrm{Re}}, \tag{21a}$$

$$v(x, y, t) = \cos(\pi x)\sin(\pi y) e^{-2\pi^2 t/\mathrm{Re}}, \tag{21b}$$

$$p(x, y, t) = \frac{1}{4}(\cos(2\pi x) + \sin(2\pi y)) e^{-4\pi^2 t/\mathrm{Re}}. \tag{21c}$$

The domain on which we define the solution is the square $[\frac{1}{4}, 2\frac{1}{4}] \times [\frac{1}{4}, 2\frac{1}{4}]$ with periodic boundary conditions. We use the second-order accurate, energy-conserving implicit Gauss method (described in [8]) with a fixed time step ($\Delta t = 10^{-1}$) for $\mathrm{Re} = 10^5$, on a coarse 20×20 grid. The simulation is run from $t = 0$ to $t = 100$, i.e., 1000 time steps. Table 1 shows the L_∞-norm of the global

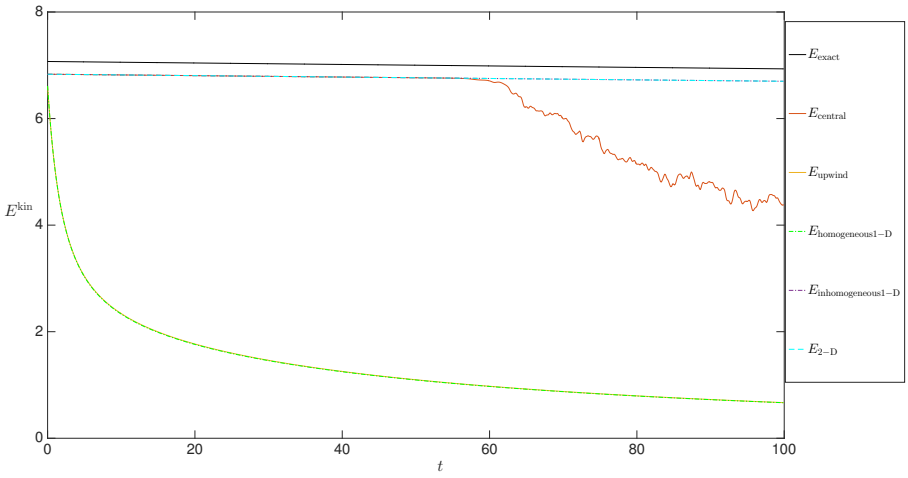

Figure 8: Temporal behavior of the discrete kinetic energy for the Taylor-Green vortex at $\text{Re} = 10^5$.

discretization error ($||e_u||_\infty = ||u_{\text{numerical}} - u_{\text{exact}}||_\infty$) for $\text{Re} = 10^5$ on a 20×20 grid at times $t = 20$ and $t = 100$, where u_{exact} is the exact velocity component computed over the grid using equation (21a). At time $t = 20$, the numerical solution obtained using the central scheme does not exhibit oscillations, and is significantly more accurate than the solutions of the upwind and homogeneous 1-D local BVP method. The central scheme and the inhomogeneous 1-D and 2-D local BVP methods appear to produce practically identical results at $t = 20$. However, at $t = 100$, the central scheme gives an oscillating solution, which severely affects the accuracy.

Figure 8 shows the dissipation of the discrete kinetic energy for all the methods applied to the Taylor-Green vortex flow. As expected, the upwind discretization shows the highest dissipation of kinetic energy. For a coarse grid and high Re (high Péclet numbers), the homogeneous 1-D local BVP method has a higher contribution from the upwind part u^{upwind} compared to the central part u^{central}, cf. equation (17). Consequently, the homogeneous 1-D local BVP method has similar dissipation of energy as the upwind scheme. The inhomogeneous 1-D and 2-D local BVP methods exhibit the same dissipation of the kinetic energy as the central scheme, until the latter breaks down (at about t = 55). The inclusion of the source term in the local BVP appears to nullify the effect of numerical dissipation from the homogeneous part. Although the central scheme results in a symmetry-preserving discretization, which is energy-conserving [9], the presence of oscillations in its numerical solution results in non-physical dissipation of energy, as observed in figure 8.

Next,we investigate the convergence of spatial errors over a family of uniform grids ranging from 5×5 to 320×320 for $\text{Re} = 100$. For this case we use

Method	$\|\|e_u\|\|_\infty$ $(t = 20)$	$\|\|e_u\|\|_\infty$ $(t = 100)$
Central	1.2419×10^{-5}	1.8592
Upwind	8.2078×10^{-1}	8.8509×10^{-1}
Homogeneous 1-D local BVP	8.2073×10^{-1}	8.8505×10^{-1}
Inhomogeneous 1-D local BVP	1.2419×10^{-5}	1.3759×10^{-4}
2-D local BVP	1.2419×10^{-5}	1.3759×10^{-4}

Table 1: Absolute errors ($||e_u||_\infty$) for the Taylor-Green vortex problem, for Re $= 10^5$ on a 20×20 grid, for $t = 20$ and $t = 100$.

the fourth-order, four-stage explicit Runge-Kutta method, just as in [10], to ensure that at sufficiently small time step the temporal errors are negligible compared to the spatial errors. Figure 9 shows the convergence of the errors ($||u_{\text{num}} - u_{\text{exact}}||_\infty$) for Re $= 100$ over a family of uniform grids, for a fixed time step $\Delta t = 10^{-3}$. It can be observed that the upwind discretization of the convective terms results in a first-order accurate scheme. The homogeneous 1-D local BVP method has a dominant upwind (u^{upwind}) contribution for coarser grids (due to higher Péclet numbers), hence exhibits first-order accuracy there. However, for finer grids (decreasing Péclet numbers), the central part (u^{central}) becomes dominant, leading to second-order convergence. The inclusion of the source terms in the local BVP improves the accuracy of the computed numerical solution significantly, resulting in the same error behavior (same order and same magnitude) as that of the central scheme.

6.2. Lid-driven cavity flow

This internal flow problem is very well suited for studying the effect of including the cross-flux term in the computation of cell-face velocity components due to the strong two-dimensionality of the flow. We investigate the lid-driven cavity flow for the case Re $= 100$, and use the results obtained by Ghia, Ghia and Shin [11] as reference solutions. We apply a pair of fairly coarse grids, viz., 8×8 and 16×16 for the Re $= 100$ case. Figures 10 and 11 show the plots of the horizontal velocity component u along the vertical center line of the cavity on the two grids. We compare the velocity profiles obtained using the central scheme, the upwind scheme and the three methods described in section 3. The upwind method yields the least accurate results, as observed from figures 10 and 11. For the 8×8 grid, we have higher Péclet numbers, thus the homogeneous 1-D local BVP method behaves much like the upwind method. The inclusion of the discrete pressure gradient in the inhomogeneous 1-D local BVP method enhances the accuracy of the homogeneous 1-D local BVP method and gives velocity profiles similar to the central scheme as observed in both figure 10

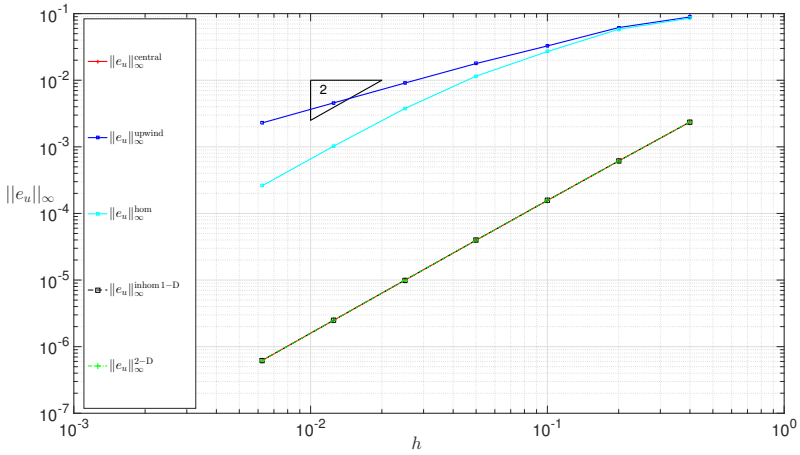

Figure 9: Convergence of the spatial errors for Taylor-Green problem for Re = 100 and $t = 20$, over a family of grids $(5 \times (2^i, 2^i),\ \ i = 0, 1, 2, 3, 4, 5, 6\ )$.

and figure 11. The 2-D local BVP method performs the best of the considered methods, primarily due to the strong two-dimensionality of the flow.

Over coarse grids the inclusion of the source terms in the local BVP for the approximation of the cell-face velocity components results in higher accuracy than the central scheme. Further, we observe that the inclusion of the source terms appears to cancel the dissipative effects arising from the upwind part of the homogeneous part of the cell-face velocity component.

7. Conclusion

In this paper we present methods for computing the cell-face velocity components involved in the discrete convective terms of the incompressible Navier-Stokes equations, using local BVPs. The cell-face velocities are computed by iteratively solving the nonlinear, local BVPs. Depending on the terms in the right-hand side of the local BVP we get three different methods, namely, the *homogeneous* 1*-D local BVP method*, the *inhomogeneous* 1*-D local BVP method* and the 2*-D local BVP method*. The homogeneous 1-D local BVP method provides an estimate for the cell-face velocity as a weighted average of the neighboring values depending on the Péclet number. In the limiting case $P \to 0$, it becomes identical to the central scheme and for $|P| \to \infty$ it reduces to the upwind scheme. The order of accuracy of the computed numerical solutions using the homogeneous 1-D local BVP method varies from first-order to second-order depending on the grid Péclet numbers.

In the inhomogeneous 1-D local BVP method we include the effect of the pressure gradient, where it is assumed that the pressure is piecewise linear. As an enhancement of the inhomogeneous 1-D local BVP method we have the 2-D

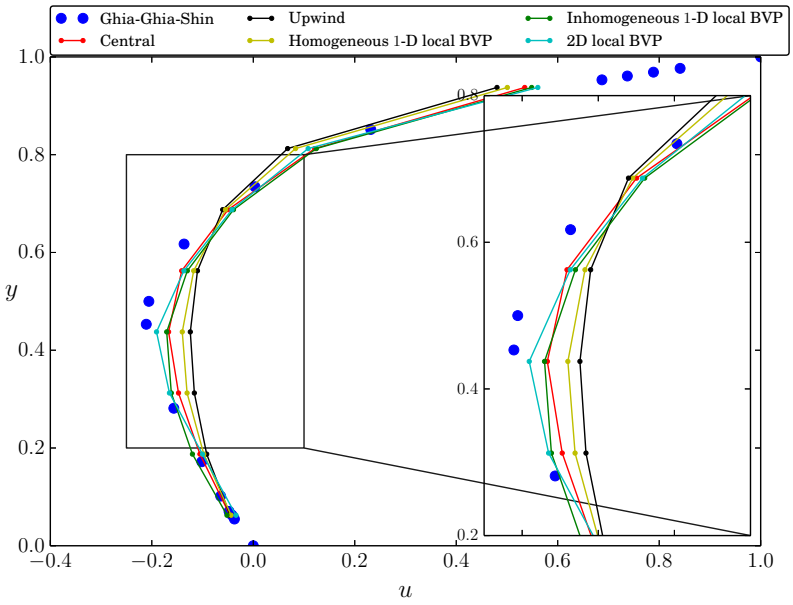

Figure 10: Horizontal velocity component along the vertical center line of the cavity for $\mathrm{Re} = 100$ on a uniform 8×8 grid.

local BVP method where we include both the pressure gradient and the cross-flux gradient. Unlike the homogeneous 1-D local BVP method, the inclusion of the source terms results in second-order accurate numerical solutions for all test cases considered. As observed for the case of the Taylor-Green problem, both the inhomogeneous 1-D local BVP method and the 2-D local BVP method exhibit perfect kinetic energy dissipation. The central scheme, which suffers from spurious oscillations, fails at higher Péclet numbers. The local BVP methods do not exhibit oscillations, which can be credited to the presence of the upwind component in the homogeneous part of the cell-face velocities.

For incompressible flows, the numerical scheme is energy conserving if the discrete convective operator is skew-symmetric, which happens only if the cell-face velocities are computed by central averaging. For the local BVP methods, the discrete convective operator is not skew-symmetric, thus the work done by the convective forces is formally not zero. Nevertheless, the inhomogeneous 1-D local BVP method and the 2-D local BVP method do not show any dissipative behavior.

Of the three local BVP methods, the 2-D local BVP method is to be preferred as it results in a more accurate approximation.

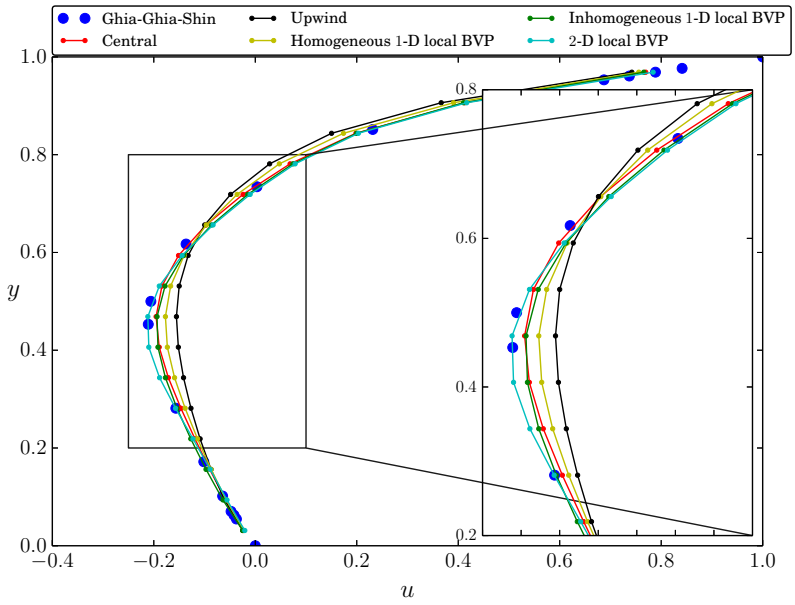

Figure 11: Horizontal velocity component along the vertical center line of the cavity for $\mathrm{Re} = 100$ on a uniform 16×16 grid.

8. Acknowledgement

This work is part of the research programme of the Foundation for Fundamental Research on Matter (FOM), which is part of the Netherlands Organization for Scientific Research (NWO).

References

[1] D. You, R. Mittal, M. Wang, P. Moin, Analysis of stability and accuracy of finite-difference schemes on a skewed mesh, Journal of Computational Physics 213 (2006) 184 – 204.

[2] M. M. Gupta, R. P. Manohar, On the use of central difference scheme for Navier-Stokes equations, International Journal for Numerical Methods in Engineering 15 (1980) 557–573.

[3] P. E. O. Buelow, S. Venkateswaran, C. L. Merkle, Stability and convergence analysis of implicit upwind schemes, Computers and Fluids 30 (2001) 961 – 988.

[4] Y. Morinishi, T. S. Lund, O. V. Vasilyev, P. Moin, Fully conservative higher order finite difference schemes for incompressible flow, Journal of Computational Physics 143 (1998) 90 – 124.

[5] S. V. Patankar, Numerical Heat Transfer and Fluid Flow, Series in Computational Methods in Mechanics and Thermal Sciences, Hemisphere Pub. Corp., 1980.

[6] D. B. Spalding, A novel finite difference formulation for differential expressions involving both first and second derivatives, International Journal for Numerical Methods in Engineering 4 (1972) 551–559.

[7] F. H. Harlow, J. E. Welch, Numerical calculation of time-dependent viscous incompressible flow of fluid with free surface, Physics of Fluids 8 (1965) 2182–2189.

[8] B. Sanderse, Energy-conserving Runge-Kutta methods for the incompressible Navier-Stokes equations, Journal of Computational Physics 233 (2013) 100 – 131.

[9] R. W. C. P. Verstappen, A. E. P. Veldman, Symmetry-preserving discretization of turbulent flow, Journal of Computational Physics 187 (2003) 343 – 368.

[10] B. Sanderse, B. Koren, Accuracy analysis of explicit Runge-Kutta methods applied to the incompressible Navier-Stokes equations, Journal of Computational Physics 231 (2012) 3041 – 3063.

[11] U. Ghia, K. N. Ghia, C. T. Shin, High-Re solutions for incompressible flow using the Navier-Stokes equations and a multigrid method, Journal of Computational Physics 48 (1982) 387–411.

PREVIOUS PUBLICATIONS IN THIS SERIES:

Number	Author(s)	Title	Month
16-17	R. Beltman J.H.M. ten Thije Boonkkamp W.L. IJzerman	A least-squares method for the inverse reflector problem in arbitrary orthogonal coordinate systems	August ‘16
16-18	I.N. Zwaan M.E. Hochstenbach	Multidirectional subspace expansion for one-parameter and multiparameter Tikhonov regularization	August ‘16
16-19	N.K. Yadav J.H.M. ten Thije Boonkkamp W.L. IJzerman	A least-squares method for the design of two-reflector optical systems	September ‘16
16-20	T.G.J. Beelen J.J. Dohmen E.J.W. ter Maten B. Tasić	Fitting generalized Gaussian distributions for process capability index	October ‘16
16-21	N. Kumar J.H.M. ten Thije Boonkkamp B. Koren	Local BVP methods for the computation of cell-face velocities in the incompressible Navier-Stokes equations	November ‘16

Ontwerp: de Tantes,
Tobias Baanders, CWI